In: Progress in Hybrid RANS-LES Modelling, NNFM, volume 117, pp. 303-314

S. Fu, W. Haase, S.-H. Peng and D. Schwamborn (editor), Springer, 2013

Hybrid RANS-LES Simulation of Turbulent High-Lift Flow in Relation to Noise Generation

Bastian Nebenführ, Shia-Hui Peng and Lars Davidson

Abstract Turbulence-resolving simulations have been performed using hybrid RANS-LES approaches for the turbulent flow around a three-element high-lift configuration. The main purpose is to explore the effect of some modeling-related numerical aspects on the simulation of resolved velocity and pressure fluctuations as potent noise-generating sources. Along with a presentation of resolved instantaneous and mean flow features, the impact of the time step and the spanwise extent of the computational domain is investigated. It is shown that the temporal resolution and the spanwise extension of the computational domain impose effects not only on the prediction of mean flow, but more significantly on the correlation of resolved turbulent structures, which may consequently affect the accuracy of flow-generated noise properties.

1 Introduction

Deploying high-lift multi-element devices during landing and takeoff triggers complex flow phenomena characterized by boundary layer transition, turbulent free shear-layers, wakes and boundary layers, as well as their confluence and interactions. At a moderate angle of attack (AoA), moreover, boundary layer separation over the flap may arise in the presence of adverse pressure gradient. High-lift flow properties are inherently connected with each other, challenging the modeling of

Bastian Nebenführ
Chalmers University of Technology, SE-412 96 Göteborg, Sweden, e-mail: basneb@chalmers.se

Shia-Hui Peng
Swedish Defence Research Agency (FOI), Stockholm, Sweden, e-mail: peng@foi.se
Chalmers University of Technology, SE-412 96 Göteborg, Sweden, e-mail: peng@chalmers.se

Lars Davidson
Chalmers University of Technology, SE-412 96 Göteborg, Sweden, e-mail: lada@chalmers.se

flow physics in numerical analysis of high-lift systems. A failure in modeling one of such phenomena may lead to overall discrepancies in the prediction of high-lift flows.

Along with the lift performance, another major concern on high-lift devices in aircraft design is that they are potent generators of airframe noise. In aeroacoustic analysis, it is known that conventional RANS methods are not suitable, since noise-generating sources in a high-lift flow are associated with unsteady flow motions in relation to extensive turbulent fluctuations. To achieve reliable predictions of aeroacoustic noise radiated from a high-lift system, turbulence-resolving modeling approaches have to be invoked.

With the rapid increase in computing power and the contemporary improvements in developing hybrid RANS-LES models, it is nowadays feasible to use turbulence-resolving methods for predicting the flow around high-lift configurations at takeoff or landing Reynolds numbers, as recently shown in Refs. [3, 10].

In the present work, the turbulent flow around a three-element airfoil is computed using a zero-equation hybrid RANS-LES model (HYB0) [8, 9]. For comparison, also a simulation with the Spalart-Allmaras Detached Eddy Simulation (SA-DES) model [13] has been performed. Since it is widely acknowledged that the slat stands for a great deal of the high-lift systems noise generation, emphasis is placed mainly on the slat cove region, when it comes to the acoustic noise source analysis. An in-depth investigation of the flow properties, in the form of spatial correlations is conducted. Also the influence of time step used in turbulence-resolving simulations is investigated.

2 Case description

The geometry under investigation is the DLR F15 three-element high-lift configuration. It consists of a leading-edge slat, a main wing and a trailing-edge flap. The same geometry has previously been studied in the LEISA project at DLR [14, 15] and is a test case in the EU-project ATAAC (Advanced Turbulence Simulation for Aerodynamic Application Challenges). All elements of the airfoil possess blunt trailing-edges, except the sharp slat cusp.

For the numerical simulations, the flow has been simulated at free flight conditions, for which the angle of attack (AoA) has been corrected to $\alpha = 6^\circ$ in precursor RANS computations by taking into account the influence of the wind tunnel side walls present in the experiment.

For turbulence-resolving simulations, the flow around the 2D high-lift configuration has to be computed in a three-dimensional domain with a certain extension in the spanwise direction, over which a uniform grid spacing is patched. The effect of the spanwise domain size on the transverse correlation of resolved turbulent structures is investigated by taking two different spans. The *small domain* has a spanwise section of 8% of the retracted chord length, C, with 40 cells, and the *large domain*

has a 16%C span with 80 cells. This yields, respectively, 8.08 and 15.96 million grid points.

Computations were carried out at $\alpha = 6^\circ$, with a freestream Mach number of $M_\infty = 0.15$ and a chord-based freestream Reynolds number of $Re_\infty \approx 2.1 \times 10^6$. Local laminar-turbulent boundary layer transition was prescribed for all three elements of the airfoil. Furthermore, two different time step sizes were used with, respectively, a *small time step* of $\Delta t = 0.001027\, C/U_\infty$ and a *large time step* of $\Delta t = 0.002054\, C/U_\infty$. Periodic boundary conditions were employed at the spanwise boundaries.

3 Results and discussion

In this section, we will first explore the resolved instantaneous flow and the mean flow features to highlight the impact of turbulence modeling and modeling-related numerical issues. It is noted here that the SA-DES computation yields similar or slightly worse predictions than the HYB0 model compared to wind-tunnel measured data. In the analysis using unsteady flow properties, we have thus taken only the results obtained with the HYB0 model, unless otherwise stated.

3.1 Resolved Instantaneous Flow and Mean Flow

In hybrid RANS-LES simulations, in spite of the fact that near-wall grid resolution in the wall-parallel plane is preferably relaxed, the modeling capability of resolving turbulent structures in off-wall LES regions relies strongly on the local grid density. Figure 1 illustrates the resolved turbulent structures in the slat cove. Detached from the slat cusp, the free shear-layer plays a significant role in the formation of the subsequent recirculating flow and the flow through the slat-wing gap. With the present grid resolution, the resolved shear-layer remains fairly stable and two-dimensional with delayed instabilities taking place at nearly half-way towards the slat-wing gap. After the shear-layer breaks down, nonetheless, the flow evolves to three-dimensional vortex motions with relatively rich structures resolved. Those are subsequently incorporated in part into the recirculating flow inside the cove and partly ejected through the slat-wing gap into the flow confluence above the main wing as longitudinally stretched flow structures. With the two different time steps, moreover, it is shown in Fig. 1 that the resolved turbulent contents are comparable.

The overall mean flow pattern around the airfoil has the appearance of a typical high-lift flow, including recirculation bubbles in the slat cove and in the cove below the main wing trailing-edge. Flow separation is observed on the suction side of the flap. Nevertheless, as shown below, a detailed exploration shows that the predicted local mean flow properties may to different extents be affected by the turbulence model, the time step and the computational domain used.

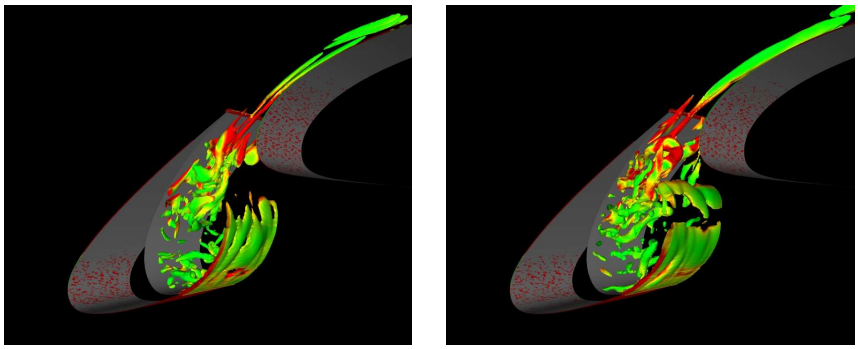

(a) *small* Δt (b) *large* Δt

Fig. 1 Isosurface of Q-invariant in the slat cove region; the structures are colored by vorticity magnitude (Computed with the HYB0 model on the small domain)

Figure 2 shows a comparison of surface pressure distributions obtained from different computations. Results from two-dimensional steady RANS simulations at $\alpha = 6^\circ$ are also included as references. The Spalart-Allmaras (SA) model [12] has under-predicted the pressure on the suction side, whereas the SST $k-\omega$ model [7] yields very good agreement with the experimental data. Of the turbulence-resolving computations, the HYB0 model with a large domain and a small time step gives the best prediction, as is highlighted further in Fig. 2(b) for the distribution around the slat. Taking the HYB0 prediction with a small domain and a large time step for a comparison, it is observed that a reduced time step has slightly improved the prediction as indicated by the distribution obtained by the same model on the same (small) domain. Keeping the small time step and using the large domain, the prediction is brought closest to the measured C_p distribution with the HYB0 model. The SA-DES result, on the other hand, gives the largest over-prediction of the surface pressure on the suction side. In view of the pressure distribution, it is illustrated in Fig. 2 that both the time step and the spanwise domain extension have played a sensible role in the prediction of surface pressures, in particular, on the suction side of the slat.

Mean velocity profiles are presented in Fig. 3 for three different locations over the boundary layer on the suction side at, respectively, the leading-edge (Fig. 3 (a)) and the trailing-edge (Fig. 3 (b)) of the main wing, and at a position close to the flap trailing-edge (Fig. 3 (c)). The general tendency in the velocity distributions, obtained with hybrid RANS-LES modeling, is similar, but variations in the predicted profiles are not insignificant. This is particularly true for the velocity profiles predicted near the flap trailing-edge, where flow separation takes place. Corresponding to the under-predicted pressure distribution as shown in Fig. 2, at $x/C = 0.09$, the SA RANS simulation has produced the largest streamwise velocity in the vicinity of the wall surface. Away from the wall, the confluence of the flows from the slat upper and lower sides after the slat trailing-edge is reflected by the kink in the velocity profile at about $y/C \approx 0.25$. Approaching the main wing trailing-edge, at $x/C = 0.88$ shown in Fig. 3(b), the hybrid RANS-LES modeling has produced smaller stream-

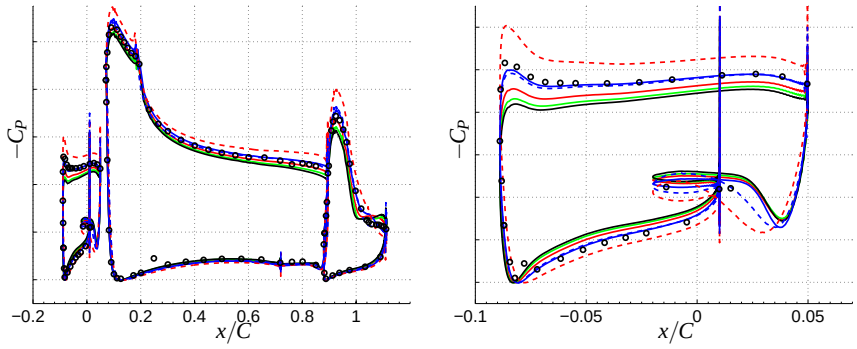

(a) all elements (b) slat only

Fig. 2 Pressure distribution around the high-lift configuration (a) and around the slat (b); ——: HYB0 (small domain, small Δt); ——: HYB0 (large domain, small Δt); ——: HYB0 (small domain, large Δt);——: SA-DES (small domain, large Δt); - - -: 2D RANS, SA model; - - -: 2D RANS, SST model; ○: Experiment.

wise velocities in the near-wall boundary layer than the 2D RANS computations. In other words, the RANS computation predicts larger values of skin friction over the wing suction side, and the turbulent diffusion is less extensive in the resolved boundary layer by the hybrid RANS-LES modeling. At $x/C = 1.08$ near the flap trailing-edge, as shown in Fig. 3(c), the SA RANS model does not capture the flow separation that was observed in the experiment, whilst the SST RANS model has predicted it reasonably well. The HYB0 and SA-DES computations are able to reproduce the flow separation over the flap trailing-edge, but the sizes of the separation bubble are different. This has been partly reflected by the different magnitudes of negative velocity in the reverse flow beneath the separation bubble. In Fig. 3, the RANS-LES interface location is also plotted (by the horizontal dashed line) for the simulations with the HYB0 model. At $x/C = 0.88$ near the main wing trailing-edge (Fig. 3(b)), the RANS-LES transition takes place inside the wall boundary layer. It is noted that, different from the SA DES model, which may suffer from the so-called "Modeled Stress Depletion (MSD)" due to such a RANS-LES interface, the HYB0 model has been viewed as being similar to a wall-modeled LES approach. A RANS-LES interface penetrating in the boundary layer is not expected to trigger any unphysical behavior in the prediction. Inspecting the ratios of the boundary layer thickness to the local grid spacing, $\delta/\Delta x$ and $\delta/\Delta z$, for the two locations on the main wing, reveals that the grid is too coarse to support LES in the boundary layer. This should not be problematic for the leading-edge position, as the entire boundary layer is treated in RANS mode, but might prove to have a negative influence on the boundary layer at the trailing-edge of the main wing, even though only the outer part of the boundary layer is actually treated by the underresolved LES.

The resolved turbulent kinetic energy, $\langle k \rangle$, in the slat cove region is depicted in Fig. 4. The contours are comparable in terms of locations of relatively high or low values of $\langle k \rangle$. Using the large time step, has, however, produced a slightly larger

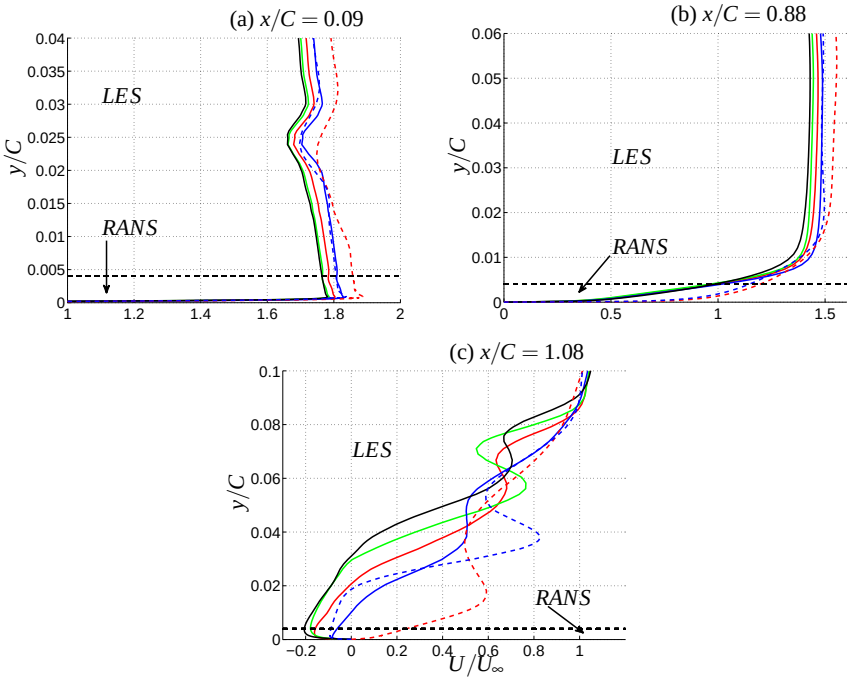

Fig. 3 Boundary layer profiles on the main wing leading-edge (a), the main wing trailing-edge (b) and on the flap (c); For legend see Fig. 2.

turbulence intensity around the impingement point of the shear-layer vortices on the lower slat surface. This has probably been induced by a more delayed and less pronounced shear-layer instability with the large time step than with the small one. The momentum inherent in the shear-layer vortices is thus less diffused with the large time step. Consequently, the impingement of the shear-layer on the slat lower surface becomes more extensive and generates relatively large turbulent energy. On the other hand, it is shown that the resolved kinetic energy levels are higher further into the recirculation bubble for the finer temporal resolution, which is expected, since more energy-bearing eddies characterized by short time scales may be resolved. For a similar high-lift configuration, experimental and numerical studies were carried out by Jenkins et al. [4], Choudhari and Khorrami [1] and Lockard and Choudhari [6]. In comparison with those results, the resolved energy intensity in the free shear-layer is much smaller here, but the overall tendency is comparable. The low resolved turbulent kinetic energy in the present computations is probably due to an insufficient grid resolution or too high levels of eddy viscosity in the slat cove area.

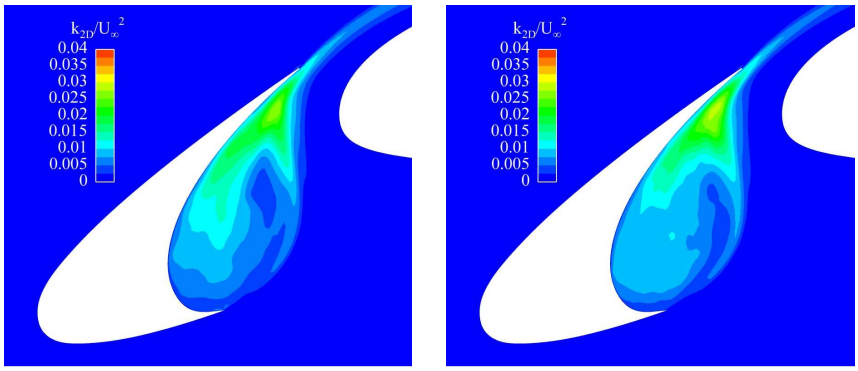

(a) *small* Δt (b) *large* Δt

Fig. 4 Resolved turbulent kinetic energy, k/U_∞^2, in the slat cove (Computed with the HYB0 model on the small domain)

(a) slat (b) flap

Fig. 5 Sampling locations around the airfoil

3.2 Spatial correlations

In relation to potential noise generation, a study of spatial correlations of pressure and velocity components is conducted. All the spanwise two-point correlations have been obtained from the HYB0 simulation with the small time step on both the small and large domains. The correlations for three selected locations in the slat cove (Fig. 5(a)) are given in Fig. 6. Moreover, the correlations for the locations around the flap (Fig. 5(b)) are presented in Fig. 7.

As presented in Fig. 6, in the slat cove region the pressure shows a strong correlation over the whole spanwise extension. Strong correlations of pressure in spanwise direction have been experienced earlier, e.g. in experiments around rectangular cylinders by Sankaran and Jancauskas [11]. The correlation of velocity fluctuations at locations S2 and S3 presents similar behavior as the pressure correlation. In general, the fluctuations of streamwise and vertical velocities show a much stronger correlation than the spanwise velocity fluctuation. It is noted here that in isotropic

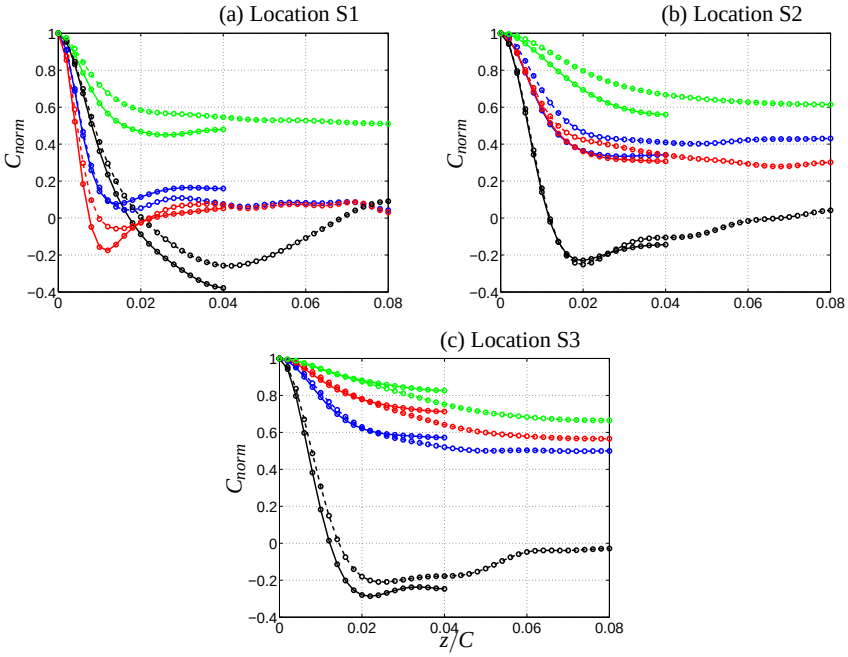

Fig. 6 Spanwise two-point correlations in the slat cove region. ——: small domain, - - - -: large domain; ——: $C_{uu,norm}$, ——: $C_{vv,norm}$, ——: $C_{ww,norm}$, ——: $C_{pp,norm}$. Markers on the lines show the resolution.

turbulence C_{ww} is twice as large as the streamwise correlations, C_{uu} and C_{vv}, which is not the case here. At point S1, which is located in the shear-layer shortly after the slat cusp, a relatively weak correlation is shown, particularly for the velocity components. From the shown correlations, one can conclude that the domain size is not sufficient in the spanwise direction even with a span of 16%C. Nonetheless, Choudhari and co-workers [1], [6] have shown that a spanwise extent of about 80% slat chord is necessary to accurately capture the major slat flow features. This corresponds to about 16%C as is used in the present work for the large domain. Correlations at locations S2 and S3 appear to be the most critical ones. A strong correlation over the whole domain in the spanwise direction at these locations can probably be attributed to the fact that they are placed in close proximity of the free shear-layer and not right in it. In these regions, the flow is undergoing an acceleration and bearing very weak turbulent energy or even tending to return to laminar flow. This may also be partly related to an insufficient grid resolution, due to which the resolved flow structures are characterized by relatively large scales and correlated over a large distance. This will be further explored in future work.

At locations F1, F2 and F3 (Fig. 5(b)), the correlation of velocity fluctuations indicates that the large domain has a sufficient spanwise size to account for all correlated turbulent structural modes. The pressure correlations at locations F1 and F2

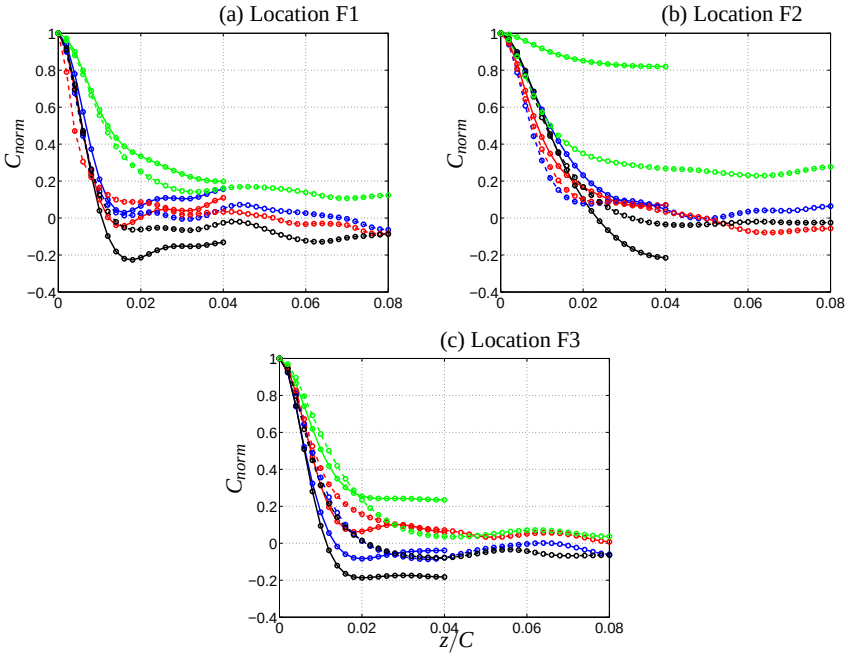

Fig. 7 Spanwise two-point correlations in the slat cove region. ——: small domain, - - - -: large domain; ——: $C_{uu,norm}$, ——: $C_{vv,norm}$, ——: $C_{ww,norm}$, ——: $C_{pp,norm}$. Markers on the lines show the resolution.

suggest that a domain with a spanwise size larger than 16%C should be preferred, however.

Moreover, the two-point correlations provide a useful measure for the spanwise resolution of the grid, as they illustrate how many cells are used to resolve the largest scales. It is shown that the correlations of the velocity components (for most locations) drop below 0.2 within 4–6 cells, which is below the minimum cell-count for a coarse LES recommended by Davidson [2].

3.3 Sound pressure level due to pressure fluctuations

In a previous work [5], the typical shape of a slat noise spectrum is presented. It shows that the highest sound levels are found at low frequencies, followed by a gradual decay for the mid-frequency region and a rather broadbanded peak at high frequencies. The high-frequency peak is attributed to vortex shedding from the blunt upper slat trailing-edge, whereas the low-frequency noise is believed to originate from shear-layer instabilities and their interactions with the solid walls in their vicinity. In Fig. 8, the Sound Pressure Level (SPL) is plotted against the Strouhal number, St, defined in terms of the slat-chord length, C_s. A generally broadband spectrum is

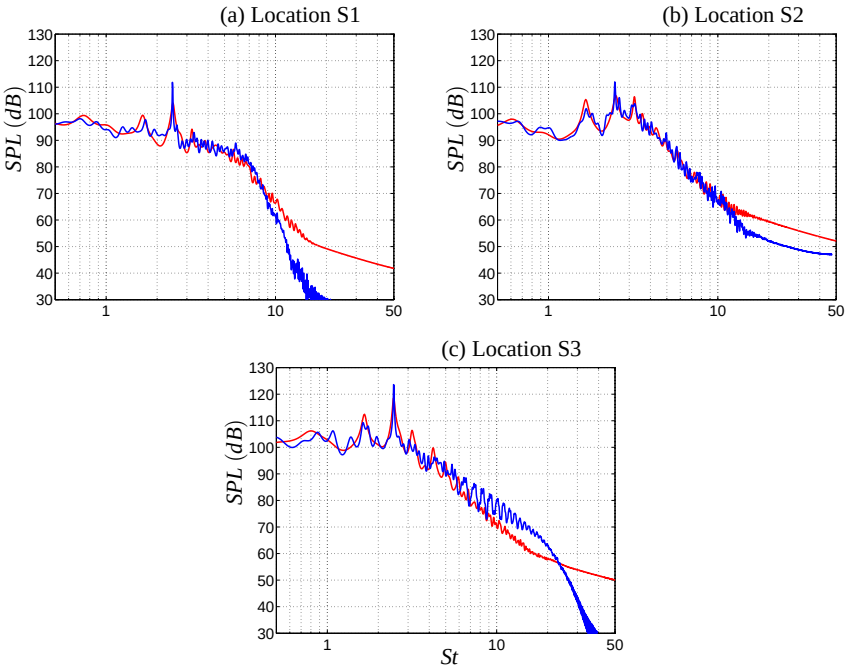

Fig. 8 Sound pressure level; ——: small Δt, ——: large Δt

shown, with the peak SPL at low Strouhal numbers. Similar spectra are obtained for both time steps. The small time step resolves the high frequencies somewhat better than the large time step. The spectrum resolved with the large time step decays relatively fast at Strouhal numbers larger than $St \approx 10$. Both time steps have produced the dominant tonal peak at identical frequency, $St \approx 2.3$, at all three sampling locations. It is believed that this frequency is associated with the shear-layer instabilities.

Besides the main tonal peak, two peaks are also present at $St \approx 1.8$ and $St \approx 3.1$, respectively. These peaks are resolved more sensibly with the small time step, and they are narrowly banded with the main peak at all locations in the cove. These may have been generated due to the interaction of the shear-layer and the solid wall. It is interesting to note that the noise source intensity increases towards the lower slat trailing-edge wall (location S3). This implies that the noise source is located around the reattachment point of the free shear-layer on that wall. Due to insufficient grid resolution around the blunt slat trailing-edge, the above mentioned broadbanded peak at high frequencies is not reproduced in the present spectral analysis.

4 Summary

The turbulent flow around the DLR F15 three-element high-lift configuration at AoA $= 6^o$ and $M_\infty = 0.15$ has been investigated using hybrid RANS-LES modeling approaches, in relation to noise-generating source analysis with an emphasis on the flow in the slat cove. The computations have been conducted with two different time steps in order to examine the effect of temporal resolution on the evolution of turbulent flow structures and, consequently, on the acoustic noise generation. Moreover, with the same cell spacing in the grid resolution, the effect of two different spans of the computational domain, with respectively a spanwise extent of 8%C and 16%C, have been assessed. The computed results are presented and compared for the mean flow and the resolved turbulent properties. Analysis of spatial correlations is performed, as well as for noise-generating sources due to unsteady flow fluctuations.

For the time-averaged mean flow, both the HYB0 model and the SA-DES model have produced reasonable results. Using a small time step and a large spanwise domain, the solution is improved particularly for the flow around the slat and for the boundary layer separation over the flap trailing-edge. This has been demonstrated with the C_p distribution on the wall surface in comparison with available experimental data. The resolved turbulent statistics have shown reasonable distributions in relation to local flow features, of which the resolved level is, however, affected by the local grid resolution.

Analysis of spatial correlations indicates a strong coherence of pressure fluctuations, over a large spanwise distance for the slat cove flow. This suggests that the spanwise extent of the computational domain should be further increased in order to better resolve the turbulent structures and to represent more accurately noise-generating sources in the slat cove. The pressure fluctuation shows usually a stronger spatial correlation than velocity fluctuations. Spanwise two-point correlations indicate that the grid resolution is not sufficient to support LES, as too few cells are used in order to resolve the largest scales.

The instability of the slat cove shear-layer is reflected in the SPL spectra that were computed using the pressure fluctuations in the slat cove. Analysis shows that the instabilities create a dominant tonal peak at $St \approx 2.3$ in the spectra. Several tonal modes can be found, which are thought to stem from the instabilities of the shear-layer and their interaction with the solid walls. Moreover, the analysis finds that the region around the slat-wing gap (including the shear-layer impingement point) is a potent noise-generating area.

In future work, computations with a refined grid will be conducted. The noise-generating source analysis will be taken by a more systematic approach on an acoustic surface using analogical methods and volumetric source terms, as well as their connection with different modes of local flow structures.

Acknowledgements

The financial support of SNIC (the Swedish National Infrastructure for Computing) for computer time at C3SE (Chalmers Center for Computational Science and Engineering) is gratefully acknowledged. This project was financed by the EU project ATAAC (Advanced Turbulence Simulation for Aerodynamic Application Challenges), Grant Agreement No. 233710. The ATAAC project is described at `http://cfd.mace.manchester.ac.uk/ATAAC/WebHome`

References

1. Choudhari, M.M., Khorrami, M.R.: Effect of Three-Dimensional Shear-Layer Structures on Slat Cove Unsteadiness. AIAA Journal. **45**, 2174–2186 (2007)
2. Davidson, L.: Large Eddy Simulations: How to evaluate resolution. International Journal of Heat and Fluid Flow. **30**, 1016–1025 (2009)
3. Deck, S.: Zonal Detached-Eddy Simulation of the Flow Around a High-Lift Configuration. AIAA Journal. **43**, 2372–2384 (2005)
4. Jenkins, L.M., Khorrami, M.R., Choudhari, M.M.: Characterization of Unsteady Flow Structures near Leading-Edge Slat: Part I. PIV Measurements. In: Proceedings of the 10th AIAA/CEAS Aeroacoustics Conference, AIAA, Manchester, UK, 10-12 May 2004
5. Khorrami, M.R.: Understanding Slat Noise Sources. In: Computational Aeroacoustics: From Acoustic Sources Modeling to Far-Field Radiated Noise Prediction - Colloquium EUROMECG 449, Chamonix, France, 9-12 December 2003
6. Lockard, D.P., Choudhari, M.M.: Noise Radiation from a Leading-Edge Slat. In: Proceedings of the 15th AIAA/CEAS Aeroacoustics Conference, AIAA, Miami, FL USA, 11-13 May 2009
7. Menter, F.R.: Two-Equation Eddy-Viscosity Turbulence Models for Engineering Applications. AIAA Journal. **32**, 1598–1605 (1994)
8. Peng, S-H.: Hybrid RANS-LES modeling based on zero- and one-equation models for turbulent flow simulation. In: Proceedings of the 4th Int. Symp. Turb. And Shear Flow Phenomena, pp. 1159-1164, Williamsburg, VA USA, 27-29 June 2005
9. Peng, S-H.: Algebraic Hybrid RANS-LES Modelling Applied to Incompressible and Compressible Turbulent Flows. In: Proceedings of the 36th AIAA Fluid Dynamics Conference and Exhibit, AIAA, San Francisco, CA USA, 5-8 June 2006
10. Peng, S-H.: Hybrid RANS-LES modeling of turbulent flow around a three-element airfoil. In: Proceedings of the 6th Int. Symp. Turb. And Shear Flow Phenomena, Seoul, South Korea, 22-24 June, 2009
11. Sankaran, R., Jancauskas, E.D.: Measurements of cross-correlation in separated flows around bluff cylinders. Journal of Wind Engineering and Industrial Aerodynamics. **49**, 279–288 (1993)
12. Spalart, P.R., Allmaras, S.R..: A One-Equation Turbulence Model for Aerodynamic Flows. In: Proceedings of the 30th Aerospace Sciences Meeting and Exhibit, Reno, NV USA, January 1992
13. Spalart, P.R., Jou, W-H., Strelets, M., Allmaras, S.R.: Comments on the feasibility of LES for wings and on a hybrid RANS/LES approach. In: Proceedings of the First AFOSR International Conference on DNS/LES, AFOSR, Rushton, LA USA, 4-8 August 1997
14. Wild, J., Pott-Pollenske, M., Nagel, B.: An integrated design approach for low noise exposing high-lift devices. In: Proceedings of the 3rd AIAA Flow Control Conference, AIAA, San Francisco, CA USA, 5-8 June 2006

15. Wild, J., Wichmann, G., Haucke, F., Peltzer, I., Scholz, P.: Large scale separation flow control experiments within the German Flow Control Network. In: Proceedings of the 47th AIAA Aerospace Sciences Meeting Including the New Horizons Forum and Aerospace Exposition, AIAA, Orlando, FL USA, 5-8 January 2009